Anisotropic lattice relaxation in non-c-plane InGaN/GaN multiple quantum wells

Junichi Nishinaka, Mitsuru Funato, and Yoichi Kawakami

Citation: Journal of Applied Physics **112**, 033513 (2012); doi: 10.1063/1.4739723
View online: http://dx.doi.org/10.1063/1.4739723
View Table of Contents: http://scitation.aip.org/content/aip/journal/jap/112/3?ver=pdfcov
Published by the AIP Publishing

Anisotropic lattice relaxation in non-*c*-plane InGaN/GaN multiple quantum wells

Junichi Nishinaka, Mitsuru Funato, and Yoichi Kawakami[a)]
Department of Electronic Science and Engineering, Kyoto University, Kyoto 615-8510, Japan

(Received 24 April 2012; accepted 27 June 2012; published online 7 August 2012)

We investigate anisotropic lattice relaxation in non-*c*-plane InGaN/GaN multiple quantum wells (MQWs). Transmission electron microscopy analyses of semipolar $(11\bar{2}2)$ MQWs reveal that lattice relaxation preferentially occurs along the $[\bar{1}\bar{1}23]$ direction by introducing misfit dislocations (MDs) with a Burgers vector of $\frac{1}{3}[11\bar{2}0]$. To theoretically describe this anisotropic relaxation phenomenon, we expand the force-balance model, where the competition between the force induced by lattice mismatch and the tension of dislocations determines the motion of dislocations. Furthermore, because MDs are introduced at the interface between the bottom InGaN QW and the underlying GaN, we propose to treat InGaN/GaN MQWs as InGaN single layers with effective In compositions. Applying this structure model to the theoretical calculation of the critical layer thicknesses reproduces well the experimentally observed lattice relaxation. This achievement enables us to design semipolar InGaN/GaN MQW structures without lattice relaxation, thereby realizing higher internal emission quantum efficiencies. © *2012 American Institute of Physics*. [http://dx.doi.org/10.1063/1.4739723]

I. INTRODUCTION

InGaN-based visible light emitters grown on semipolar and nonpolar GaN substrates have attracted much attention, because the reduction of internal electric fields induced by piezoelectric and spontaneous polarizations has been predicted theoretically[1,2] and proven experimentally.[3–6] In fact, high performance light emitting diodes (LEDs) on the semipolar $\{11\bar{2}2\}$ GaN substrates[7,8] and green laser diodes (LDs) on semipolar $\{2\bar{2}01\}$ GaN substrates[9] have already been demonstrated.

Irrespective of growth planes, it is essential to avoid lattice relaxation because misfit dislocations (MDs) induced by lattice relaxation may act as nonradiative recombination centers and prevent high performance light emission. So far, lattice relaxation phenomena have extensively been discussed for conventional polar (0001) plane,[10–13] semipolar $(11\bar{2}2)$ plane,[14,15] $(2\bar{2}01)$ plane,[15,16] $(1\bar{1}01)$ plane,[17] and nonpolar $(1\bar{1}00)$ plane.[18] The reported primary slip planes, Burgers vectors, and dislocation line directions are summarized in Table I and Fig. 1, which are discussed in more detail below.

A particularly important parameter in describing the lattice relaxation is the critical layer thickness (CLT). To date, CLT models have been established for isotropic material systems,[19–21] which include zinc blende (001) and (111) planes. However, for anisotropic material systems such as the wurtzite structure, the development of CLT models is under progress. For example, Holec *et al*. recently investigated InGaN single layers grown on wurtzite (0001) GaN with a strict consideration of the anisotropic crystal structure.[11,12] It should be noted that the (0001) plane is an isotropic plane in the anisotropic wurtzite structure. Romanov *et al*. have examined CLTs of anisotropic semipolar InGaN and AlGaN single layers.[15] However, they adopted an isotropic approximation by using averaged Poisson's ratio. Therefore, to precisely calculate the CLTs, the model without isotropic approximation is required.

Furthermore, CLTs have experimentally been demonstrated only for InGaN and AlGaN single layers as well as single quantum wells (SQWs), but have not been clarified for multiple quantum wells (MQWs), though they are more widely used for active layers in light emitters. This is because the lattice relaxation in MQWs is not as simple as that in single layers including SQWs; for example, it is still unclear for any crystal orientations as to where MDs are induced under the presence of many InGaN/GaN interfaces.

In this study, we demonstrate anisotropic lattice relaxation experimentally in InGaN/GaN MQWs grown on semipolar $(11\bar{2}2)$ GaN substrates. To describe the observation theoretically, the conventional CLT model is expanded to anisotropic growth planes in anisotropic crystal structures. In addition, based on transmission electron microscopy (TEM) observations that MDs are induced at the interface between the first InGaN QW of MQWs and the underlying GaN, we propose to treat InGaN/GaN MQWs as InGaN single layers with equivalent In compositions. In fact, this model with the developed CLT model can reproduce the anisotropic lattice relaxation in $(11\bar{2}2)$ InGaN/GaN MQWs. Finally, in order to confirm an advantage of the appropriate design of MQW structures, internal quantum efficiencies (IQEs) are compared between coherently grown and strain-relaxed InGaN QWs.

II. EXPERIMENTS

The samples used in this study were grown by metal-organic vapor phase epitaxy. The substrates were the

a)E-mail: kawakami@kuee.kyoto-u.ac.jp.

TABLE I. Primary slip planes, MD line directions, Burgers vectors, and stresses used in the calculation of CLTs for the various growth planes of wurtzite structure.

Growth plane	Polar[10] (0001)	Semipolar[15] $(11\bar{2}m)$	Semipolar[15] $(1\bar{1}0n)$	Nonpolar[18] $(1\bar{1}00)$
Primary slip plane	$\{11\bar{2}2\}$	(0001)		$(10\bar{1}0)$ $(0\bar{1}10)$
MD line direction	$\langle 1\bar{1}00\rangle$	$[1\bar{1}00]$	$[11\bar{2}0]$	[0001]
Burgers vector	$1/3\langle\bar{1}\bar{1}23\rangle$	$1/3[11\bar{2}0]$	$1/3[1\bar{2}10]$ $1/3[\bar{2}110]$	$1/3[1\bar{2}10]$ $1/3[\bar{2}110]$
b	$\sqrt{a^2+c^2}$	a	a	a
b_s	0	0	$a/2$	0
$b_{e\perp}$	a	a	$\sqrt{3}a/2$	a
$b_{e\parallel}$	c	0	0	0
K_s		$\sqrt{\frac{C_{44}(C_{11}-C_{12})}{2}}$		C_{44}
K_e $K_{e\perp}$		$(\sqrt{C_{11}C_{33}}+C_{13})\sqrt{\frac{C_{44}(\sqrt{C_{11}C_{33}}-C_{13})}{C_{33}(\sqrt{C_{11}C_{33}}+C_{13}+2C_{44})}}$		$\frac{C_{11}^2-C_{12}^2}{2C_{11}}$
K_e $K_{e\parallel}$		$(\sqrt{C_{11}C_{33}}+C_{13})\sqrt{\frac{C_{44}(\sqrt{C_{11}C_{33}}-C_{13})}{C_{11}(\sqrt{C_{11}C_{33}}+C_{13}+2C_{44})}}$		
Stress	$\sigma_{xx}=\sigma_{yy}$	$\sigma_{x'x'}$	$\sigma_{x'x'}$	$\sigma_{y'y'}$

semipolar $(11\bar{2}2)$ GaN substrates sliced from [0001]-oriented GaN crystals grown by hydride vapor phase epitaxy. The surfaces of the substrates were chemically mechanically polished. Initially, 2-μm-thick GaN homoepitaxial layers were grown on the substrates, and then, InGaN single layers, InGaN/GaN SQWs, or MQWs with various In compositions and thicknesses were grown. All samples were nominally undoped.

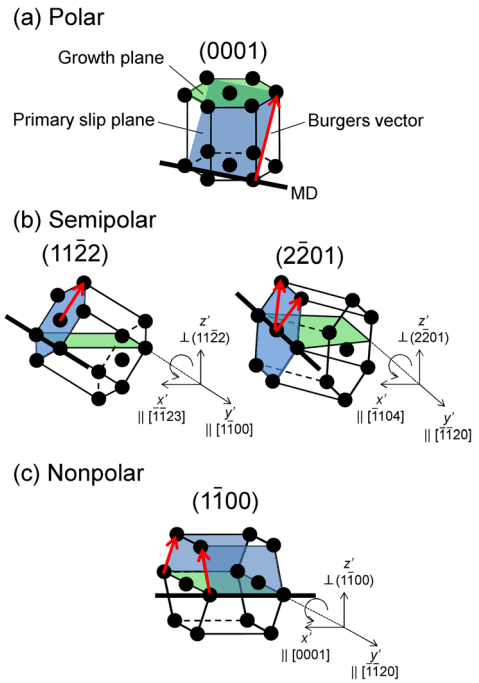

FIG. 1. The primary slip systems and the coordinate systems for (a) polar, (b) semipolar, and (c) nonpolar growth planes of a wurtzite crystal structure. Arrows and thick lines indicate the Burgers vectors and MD lines, respectively.

In compositions and QW thicknesses were evaluated by x-ray diffraction (XRD) radial scans for the $(11\bar{2}2)$ symmetric plane. To determine the In compositions of the strained $(11\bar{2}2)$ InGaN layers, we used the strain model proposed by Funato *et al.*[22] A fluorescence microscope with a 100× objective lens was used to observe the luminescence morphology. The 405 nm line of a mercury lamp was used to selectively excite the InGaN QWs. In order to observe MDs, cross-sectional TEM was performed by using a JEOL JEM-2100 F electron microscope with an acceleration voltage of 200 kV. TEM specimens were prepared by mechanical polishing and subsequent Ar ion milling.

III. EXPERIMENTAL OBSERVATIONS OF ANISOTROPIC LATTICE RELAXATION

To assess the lattice relaxation in $(11\bar{2}2)$ InGaN/GaN MQWs, we performed XRD reciprocal space mappings (RSMs) for the $(02\bar{2}2)$ and the $(11\bar{2}4)$ asymmetric planes, which reveals the coherency of the crystal lattice in the $[1\bar{1}00]$ (y' in Fig. 1(b)) and the $[\bar{1}\bar{1}23]$ (x' in Fig. 1(b)) direction, respectively. The experimental results of relaxed samples indicated that the crystal lattice of InGaN was relaxed for the $(11\bar{2}4)$ plane, and coherent for the $(02\bar{2}2)$ plane, which means that the crystal lattice was preferentially relaxed along the $[\bar{1}\bar{1}23]$ (x' in Fig. 1(b)) direction, similar to Ref. 14. XRD-RSMs for the $(11\bar{2}2)$ symmetric plane with the beam condition along $[1\bar{1}00]$ or $[\bar{1}\bar{1}23]$ confirmed that the lattice relaxation caused a crystal tilt in the InGaN layer around the $[1\bar{1}00]$ axis. This direction corresponds to the dislocation lines, as experimentally shown by TEM below. Therefore, these results suggest that the lattice is anisotropically relaxed with the introduction of MDs along the in-plane $[1\bar{1}00]$

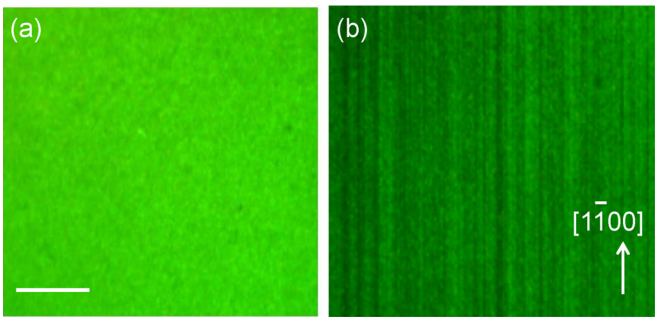

FIG. 2. Fluorescence microscope images of (a) coherently grown and (b) strain-relaxed InGaN QWs on the $(11\bar{2}2)$ GaN substrates. The scale bar represents 10 μm.

direction, and consequently, tilts around them. Thus, observing crystal tilt reveals whether the lattice is relaxed or not.

Furthermore, we revealed that the lattice relaxation affects fluorescence images. Figures 2(a) and 2(b) show fluorescence microscope images of coherently grown and strain-relaxed InGaN QWs, respectively, grown on the semipolar $(11\bar{2}2)$ GaN substrates. The coherently grown InGaN QW shows spatially homogeneous luminescence, whereas the strain-relaxed InGaN QW shows dark lines along the $[1\bar{1}00]$ direction. These lines may be related to MDs, because their direction was the same as that of dislocation lines, as discussed in TEM analyses. Thus, we distinguished coherently grown samples from strain-relaxed samples by the dark lines along the $[1\bar{1}00]$ direction as well as the crystal tilts observed by XRD measurements.

To discuss the lattice relaxation in the semipolar $(11\bar{2}2)$ InGaN/GaN heterostructures in more detail, we have to know the structure of MDs and where they are formed. For these purposes, cross-sectional TEM measurements were performed on a $(11\bar{2}2)$ InGaN/GaN SQW and a three-period MQW with almost the same In composition (~12%), QW thickness (~7 nm), and GaN barrier thickness (~9 nm).

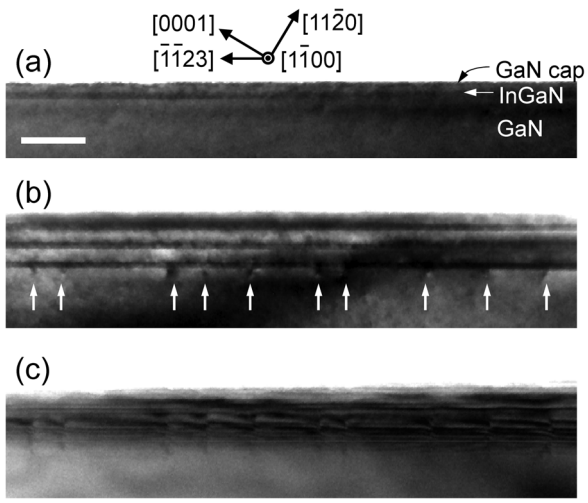

FIG. 3. Cross-sectional TEM images of (a) InGaN/GaN SQW and (b) three-period MQW grown on the semipolar $(11\bar{2}2)$ GaN substrates, viewed along the $[1\bar{1}00]$ axis. (c) That of the three-period MQW tilted about the $[\bar{1}\bar{1}23]$ axis. Arrows indicate misfit dislocations. The scale bar represents 50 nm.

Figures 3(a) and 3(b) show their cross-sectional bright-field TEM images, viewed along the $[1\bar{1}00]$ direction. The SQW shows no MDs, whereas the MQW shows an array of MDs only at the interface between the first strained InGaN QW and the underlying GaN. These results suggest that even if the thickness of each QW does not exceed the CLT, MDs can form when the total thickness of MQW exceeds a certain threshold, which for MQW is the CLT as discussed below.

Additionally, the Burgers vector of MDs was determined to be $\frac{1}{3}[11\bar{2}0]$, from a $\mathbf{g}\cdot\mathbf{b}$ invisibility analysis with the two beam condition of $\mathbf{g} = 0002$ (not shown). Figure 3(c) shows the cross-sectional TEM image of the same sample as in Fig. 3(b), but in this particular case, the TEM specimen was tilted around the $[\bar{1}\bar{1}23]$ (x') axis to see how MDs were lying at the interface. As a result, the dislocation lines were observed to be perpendicular to the $[\bar{1}\bar{1}23]$ (x') direction, and therefore, parallel to the $[1\bar{1}00]$ (y') direction. Thus, the observed MDs were determined to be pure edge dislocations. By considering the Burgers vector and the line direction of MDs, we determined the slip plane to be the (0001) plane. These results for the MDs in $(11\bar{2}2)$ InGaN/GaN MQWs will be used in theoretical calculation of CLTs in Sec. IV.

IV. THEORETICAL CLT MODELS

A. General expression

Before discussing practical cases, let us discuss the general expression of CLTs. To calculate the CLTs, we adopted the force-balance model,[19,21] where the balance of forces acting on the threading dislocations, i.e., the force due to lattice mismatch and the line tension (referred to as the "self-stress" in the Fischer model[21]), is considered. This model is based on the idea that threading dislocations pre-existing in the substrates propagate within the heterointerfaces, when the strained layer thickness exceeds the CLTs, h_c. The general equation for CLTs based on this model can be expressed as

$$\sigma b h_c \cos\lambda = \frac{1}{4\pi}\left(K_s b_s^2 + K_e b_e^2\right)\ln\left(\frac{h_c}{r_0}\right), \qquad (1)$$

where the left-hand side represents the force due to lattice mismatch acting on the slip plane, and the right-hand side corresponds to the dislocation line tension equivalent to the dislocation energy per unit length.[23] Here, σ is the in-plane stress induced by lattice mismatch, b is the length of the Burgers vector, and λ is the angle between the Burgers vector and the direction in the interface, normal to the dislocation line. Moreover, b_s and b_e are the screw and the edge components of Burgers vector, respectively, and K_s and K_e are the respective coefficients and referred to as "energy coefficients."[24] In addition, r_0 is the dislocation core radius, typically taken to be from $b/4$ to b.[24]

The CLT models have been developed for isotropic material systems, such as zinc blende (001) heterostructures. In this study, however, the anisotropy has to be taken into account, because the wurtzite structure, which is the most stable structure for nitride semiconductors, is anisotropic,

and furthermore, semipolar and nonpolar planes have in-plane anisotropy unlike the polar (0001) plane. In Secs. IV B and IV C, we demonstrate the practical expressions of CLTs for the various cases.

B. Isotropic crystal structures

1. Isotropic growth planes

As the simplest case, we first consider the isotropic growth plane in the isotropic crystal structure such as the zinc blende (001) and (111) planes. For such structures, the CLT models have been established by Matthews and Blakeslee[19] or Fischer *et al.*,[21] which, in this article, are referred to as the "M-B model" and the "Fischer model," respectively. In this case, σ, K_s, K_e, b_s, and b_e can be expressed as $\sigma = 2G\varepsilon(1+\nu)/(1-\nu)$, $K_s = G$, $K_e = G/(1-\nu)$, $b_s = b\cos\alpha$, and $b_e = b\sin\alpha$, respectively, where G is the shear modulus, ν is the Poisson's ratio, ε is the in-plane strain due to lattice mismatch, and α is the angle between the Burgers vector and the MD line direction.[23,24] By setting $r_0 = b/\mathrm{e}$ (e: base of natural logarithm), Eq. (1) can be transformed to the equation proposed by Matthews and Blakeslee[19]:

$$h_c = \frac{b(1-\nu\cos^2\alpha)}{8\pi\varepsilon(1+\nu)\cos\lambda}\left\{\ln\left(\frac{h_c}{b}\right)+1\right\}. \tag{2}$$

In the Fischer model, the stress term was modified in order to satisfy the condition that no forces can act on the free surface[21,25]:

$$\sigma' = 2G\frac{1+\nu}{1-\nu}\left(\varepsilon - \frac{b\cos\lambda}{2h_c}\right). \tag{3}$$

Then, by substituting σ' for σ and by setting $r_0 = b$ in Eq. (1), we obtain the equation of CLTs proposed by Fischer *et al.*[21]:

$$h_c = \frac{b\cos\lambda}{2\varepsilon}\left\{1+\frac{1-\nu\cos^2\alpha}{4\pi(1+\nu)\cos^2\lambda}\ln\left(\frac{h_c}{b}\right)\right\}. \tag{4}$$

2. Anisotropic growth planes

For the anisotropic growth plane such as the zinc blende (110) plane, Eqs. (3) and (4) are not applicable, because σ cannot be expressed in the same way as above. To determine σ, we have to know how the lattice relaxes and which direction of stress should be considered. Details of calculating anisotropic σ are described in Sec. IV C 2.

C. Anisotropic crystal structures

In this section, we consider anisotropic crystal structures, for which the parameters mentioned above become more complicated. For the wurtzite crystal structure, elastic properties perpendicular and parallel to the c-axis are different, so that the Burgers vectors should be decomposed into the two characteristic directions. It should be noted that the MD line direction of primary slip systems in the wurtzite structure is perpendicular (polar and semipolar) or parallel (nonpolar) to the c-axis, as illustrated in Fig. 1. Therefore, for the screw component of a Burgers vector b_s, which is parallel to the dislocation line, there is no need to include anisotropy. Similarly, for the dislocation parallel to the c-axis (nonpolar), the edge component b_e, which is perpendicular to the dislocation line, does not have to be decomposed, because elastic properties around the dislocation line, that is, within the basal (0001) plane, are isotropic.

For the dislocation perpendicular to the c-axis (polar and semipolar), the edge component of a Burgers vector b_e should be decomposed into components perpendicular, $b_{e\perp}$, and parallel to the c-axis, $b_{e||}$. Additionally, the respective energy coefficients are defined as $K_{e\perp}$ and $K_{e||}$. Applying this procedure, Eq. (1) can be rewritten as

$$\sigma b h_c\cos\lambda = \frac{1}{4\pi}(K_s b_s^2 + K_{e\perp}b_{e\perp}^2 + K_{e||}b_{e||}^2)\ln\left(\frac{h_c}{r_0}\right). \tag{5}$$

For anisotropic crystal structures, the energy coefficients K_s, $K_{e\perp}$, and $K_{e||}$ depend on the dislocation line direction.[24,26]

1. Isotropic growth plane: Polar (0001) plane

For the wurtzite (0001) plane, which is isotropic, the in-plane stress σ due to lattice mismatch can be expressed as[11,12]

$$\sigma = \sigma_{xx} = \sigma_{yy} = \frac{(C_{11}+C_{12})C_{33} - 2C_{13}^2}{C_{33}}\varepsilon. \tag{6}$$

Note that using $G = (C_{11}-C_{12})/2$ and $\nu = (C_{12}C_{33}-C_{13}^2)/(C_{11}C_{33}-C_{13}^2)$, Eq. (6) can be transformed to $\sigma = 2G\varepsilon(1+\nu)/(1-\nu)$, which holds for isotropic planes. Here, C_{ij} are the elastic stiffness coefficients.

It is noteworthy that the definitions of G and ν depend on the directions of stress and consequent lattice elastic distortion. In the case of heteroepitaxy, the elastic deformation in the growth plane should be considered. Therefore, there is a set of definitions appropriate for the plane of the interest. For the (0001) plane, the definitions given above hold, but other planes possess other definitions.

For the polar (0001) InGaN single layers on GaN, it has been reported that the MD lines were in the (0001) plane,[10] as illustrated in Fig. 1(a). In such a situation, K_s, $K_{e\perp}$, and $K_{e||}$ can be expressed as follows[24,26]:

$$K_s = \sqrt{\frac{C_{44}(C_{11}-C_{12})}{2}}, \tag{7}$$

$$K_{e\perp} = (\sqrt{C_{11}C_{33}}+C_{13})\sqrt{\frac{C_{44}(\sqrt{C_{11}C_{33}}-C_{13})}{C_{33}(\sqrt{C_{11}C_{33}}+C_{13}+2C_{44})}}, \tag{8}$$

$$K_{e||} = (\sqrt{C_{11}C_{33}}+C_{13})\sqrt{\frac{C_{44}(\sqrt{C_{11}C_{33}}-C_{13})}{C_{11}(\sqrt{C_{11}C_{33}}+C_{13}+2C_{44})}}. \tag{9}$$

According to the previous report,[10] the Burgers vector components are $b_s = 0$, $b_{e\perp} = a$, and $b_{e\parallel} = c$.

Holec *et al.* calculated CLTs for the wurtzite (0001) InGaN/GaN heterostructures with a consideration of anisotropic crystal structure,[11,12] based on the M-B model, although the coefficients were not explicitly expressed as Eqs. (7)–(9).

2. Anisotropic growth planes

The semipolar and nonpolar planes can be determined by tilting the *c*-axis of wurtzite crystal around a certain axis in the basal (0001) plane. To express anisotropy within the interfaces, the coordinates are defined for the semipolar and nonpolar planes, as shown in Fig. 1; y' is the rotation axis, x' is the direction perpendicular to y' direction in the growth plane, and z' is the direction normal to the growth plane. For example, in the semipolar $(11\bar{2}2)$ plane, x' and y' are parallel to the $[\bar{1}\bar{1}23]$ and the $[1\bar{1}00]$ direction, respectively. However, x' and y' in the $(2\bar{2}01)$ plane are the $[\bar{1}104]$ and the $[11\bar{2}0]$, respectively. To reflect the anisotropic lattice relaxation, the in-plane stress $\sigma_{x'x'}$ or $\sigma_{y'y'}$ should be chosen based on the experimental observation.

Although σ is often expressed with Poisson's ratio ν and shear modulus G as discussed in Sec. IV B 1, these parameters for the semipolar and nonpolar planes cannot be expressed in the same way as those for an isotropic growth plane without any approximation. Therefore, in this study, we directly calculate the in-plane stress using Ref. 22, without using ν and G.

a. Semipolar $(11\bar{2}m)$ *and* $(1\bar{1}0n)$ *planes.* To accurately calculate the CLTs of anisotropic growth planes such as semipolar ones, the force-balance model can be extended by considering anisotropic lattice relaxation. (A similar treatment is necessary for the anisotropic growth plane of the isotropic crystal structure.) For semipolar InGaN/GaN heterostructures, only the stress in the x' direction ($\sigma_{x'x'}$ in Ref. 22) should be included in the calculation of CLTs, because the lattice relaxation occurs preferentially in this direction, as discussed in Sec. III.

Substituting $\sigma_{x'x'}$ into σ in Eq. (5), the CLT equation based on the M-B model, including the anisotropy of crystal structure and growth plane can be obtained:

$$\sigma_{x'x'} b h_c \cos\lambda = \frac{1}{4\pi}\left(K_s b_s^2 + K_{e\perp} b_{e\perp}^2 + K_{e\parallel} b_{e\parallel}^2\right)\left\{\ln\left(\frac{h_c}{b}\right) + 1\right\}. \tag{10}$$

The relation between the stress $\sigma_{x'x'}$ and the strain $\varepsilon_{x'x'}$ and $\varepsilon_{y'y'}$ is given by

$$\sigma_{x'x'} = \frac{S'_{22}\varepsilon_{x'x'} - S'_{12}\varepsilon_{y'y'}}{S'_{11}S'_{22} - S'^2_{12}}, \tag{11}$$

where

$$S'_{11} = S_{11}\cos^4\theta + S_{33}\sin^4\theta + \frac{2S_{13} + S_{44}}{4}\sin^2 2\theta, \tag{12}$$

$$S'_{22} = S_{11}, \tag{13}$$

$$S'_{12} = S_{12}\cos^2\theta + S_{13}\sin^2\theta, \tag{14}$$

based on the Hooke's law.[27] Here, S_{ij} are the elastic compliances, which can be calculated from the elastic stiffness coefficients C_{ij}, and θ is the rotation angle with respect to the (0001) plane. Note that Eq. (11) can also be written with C_{ij}, as Eq. (6), but S_{ij} can provide a simpler expression. In addition, $\varepsilon_{x'x'}$ and $\varepsilon_{y'y'}$ are the in-plane strains due to lattice mismatch in the x' and the y' directions, respectively, as detailed in Ref. 22. K_s, $K_{e\perp}$, and $K_{e\parallel}$ are given by Eqs. (7)–(9).

Fischer *et al.* proposed to modify the stress term in order to satisfy the free surface condition, as shown in Eq. (3). In this study, we assumed that only the strain in the x' direction was partially relieved by the effect of the free surface, because the MDs were lying along the y' direction. Using $\sigma_{x'x'}$ for σ again, and setting $r_0 = b$, the equation of CLTs for the semipolar plane based on the Fischer model can be extracted:

$$\left(\sigma_{x'x'} - \frac{S'_{22} b\cos\lambda/2h_c}{S'_{11}S'_{22} - S'^2_{12}}\right) b h_c \cos\lambda = \frac{1}{4\pi}\left(K_s b_s^2 + K_{e\perp} b_{e\perp}^2 + K_{e\parallel} b_{e\parallel}^2\right)\ln\left(\frac{h_c}{b}\right). \tag{15}$$

Note that although the equation was described as the balance of "force," unlike the original expression based on the "stress" equilibrium,[21] these models are essentially identical.

For the semipolar $(11\bar{2}2)$ InGaN/GaN heterostructures, we have experimentally confirmed that the MD lines were parallel to the $[1\bar{1}00]$ direction, and their Burgers vectors were $\frac{1}{3}[11\bar{2}0]$ as demonstrated in Sec. III. Therefore, we determined that $b = b_{e\perp} = a$, and λ is equal to the angle between the $(11\bar{2}2)$ plane and the (0001) plane (for example, 58.4° for GaN and 58.1° for InN), as summarized in Table I.

For the $(2\bar{2}01)$ InGaN/GaN heterostructures, it has been reported that the MD lines were parallel to the $[11\bar{2}0]$ direction, and their Burgers vectors were $\frac{1}{3}[1\bar{2}10]$ or $\frac{1}{3}[\bar{2}110]$.[15] Therefore, the Burgers vector components are $b_s = a/2$, $b_{e\perp} = \sqrt{3}a/2$, and $b_{e\parallel} = 0$.

b. Nonpolar $(1\bar{1}00)$ *plane.* For the nonpolar $(1\bar{1}00)$ plane, the MD lines are parallel to the [0001] direction, different from other planes, where the MD lines are lying in the (0001) plane. Their Burgers vectors are $\frac{1}{3}[1\bar{2}10]$ or $\frac{1}{3}[\bar{2}110]$.[18] Therefore, $b = b_e = a$. Teutonico *et al.* have calculated the energy coefficients for an infinitely straight dislocation propagating along the [0001] direction[26]:

$$K_s = C_{44}, \tag{16}$$

$$K_e = \frac{C_{11}^2 - C_{12}^2}{2C_{11}}. \tag{17}$$

If we taking into account the anisotropic lattice relaxation preferentially occurring in the y' direction, we should substitute $\sigma_{y'y'}$ into Eq. (5). Therefore, the equation of the extended M-B model for the nonpolar $(1\bar{1}00)$ plane can be obtained:

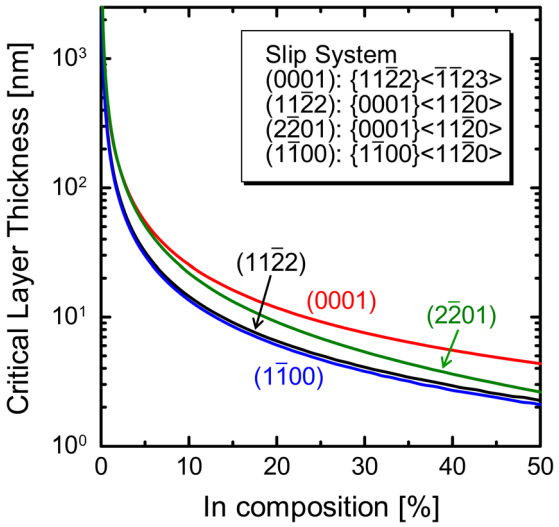

FIG. 4. Calculated CLTs based on the extended Fischer model [Eq. (15)] for InGaN single layers grown on various planes.

$$\sigma_{y'y'} b h_c \cos\lambda = \frac{1}{4\pi}(K_s b_s^2 + K_e b_e^2)\left\{\ln\left(\frac{h_c}{b}\right) + 1\right\}, \quad (18)$$

where $\sigma_{y'y'}$ can be written as functions of $\varepsilon_{y'y'}$ and $\varepsilon_{x'x'}$:

$$\sigma_{y'y'} = \frac{S'_{11}\varepsilon_{y'y'} - S'_{12}\varepsilon_{x'x'}}{S'_{11}S'_{22} - S'^2_{12}}, \quad (19)$$

S'_{11}, S'_{12}, and S'_{22} are given in Eqs. (12)–(14).

On the other hand, adopting similar treatment as Eq. (15), the equation of the extended Fischer model for the nonpolar $(1\bar{1}00)$ plane can be obtained:

$$\left(\sigma_{y'y'} - \frac{S'_{11} b \cos\lambda / 2h_c}{S'_{11}S'_{22} - S'^2_{12}}\right) b h_c \cos\lambda = \frac{1}{4\pi}(K_s b_s^2 + K_e b_e^2)\ln\left(\frac{h_c}{b}\right). \quad (20)$$

3. Calculation of CLTs for various growth planes

Figure 4 compares the theoretical CLT values of InGaN single layers on GaN among the polar (0001), the semipolar $(11\bar{2}2)$, $(2\bar{2}01)$, and the nonpolar $(1\bar{1}00)$ growth planes, based on the extended Fischer model. The lattice parameters and the elastic stiffness constants for GaN and InN are listed in Table II.[28] For $In_xGa_{1-x}N$, these parameters were interpolated linearly by the In composition x. Burgers vectors, energy coefficients and stresses are summarized in Table I.

TABLE II. Material parameters used for the calculation of CLTs.[28]

Parameters	GaN	InN
a at 300 K (nm)	0.3189	0.3545
c at 300 K (nm)	0.5185	0.5703
C_{11} (GPa)	390	223
C_{12} (GPa)	145	115
C_{13} (GPa)	106	92
C_{33} (GPa)	398	224
C_{44} (GPa)	105	48

It should be noted that applicable model, that is, the lattice relaxation mechanism depends on the growth plane, growth condition, or threading dislocation density. As demonstrated below, the extended Fischer model can well account for the experimental results of $(11\bar{2}2)$ InGaN on GaN. For the polar (0001) plane, however, it has been reported that the measured CLTs are much lower than those predicted by the extended Fischer model, and almost agree with those of the M-B model.[11,12] The observed difference in the $(11\bar{2}2)$ and (0001) InGaN may be related to generation mechanisms of dislocations; in the InGaN/GaN MQW grown on a (0001) GaN substrate, dislocation pairs were generated from InGaN/GaN interfaces,[13] whereas this situation does not necessarily occur for other crystallographic planes.

V. RESULTS AND DISCUSSION

A. Comparison between experimental results and theoretical models

Figure 5(a) shows lattice relaxation phenomena in $(11\bar{2}2)$ InGaN single layers and SQWs. Open circles and crosses indicate coherently grown and strain-relaxed samples, respectively, which were experimentally confirmed by the methods described in Sec. III. The dashed and solid lines indicate the CLTs for the semipolar $(11\bar{2}2)$ InGaN single

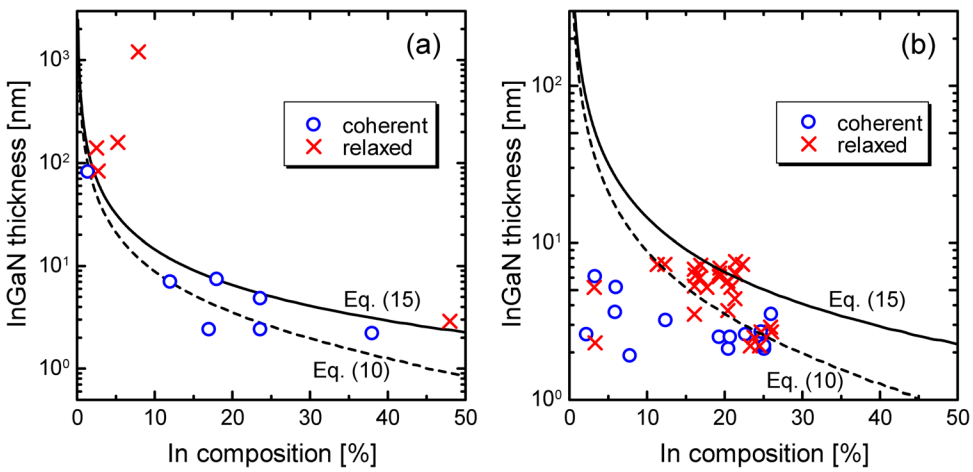

FIG. 5. Theoretical and experimental assessment of strain relaxation for (a) InGaN single layers and SQWs, and (b) InGaN/GaN MQWs. Solid and dashed lines are the CLTs calculated with Eqs. (15) and (10), respectively. Open circles and crosses are for coherently grown and strain-relaxed samples, respectively.

layer theoretically calculated by Eq. (10) based on the M-B model and Eq. (15) based on the Fischer model, respectively. As shown in Fig. 5(a), the theoretical calculation based on Eq. (15) was in good agreement with experimental results. This result suggests that the free surface plays a role in lattice relaxation of $(11\bar{2}2)$ InGaN/GaN.[21,25]

Moreover, Hsu *et al*. reported that a 40-nm-thick InGaN single layer with In composition of 1% grown on the $(11\bar{2}2)$ GaN substrate was coherent, whereas those with In composition of 4%, 5%, and 6% were relaxed.[29] These results also agree with Eq. (15).

In contrast, the lattice relaxation phenomena in $(11\bar{2}2)$ InGaN/GaN MQWs cannot be reproduced by the theoretical calculations as demonstrated in Fig. 5(b), where experimental results are plotted as functions of In composition and QW thickness for each QW. It should be noted that each QW thickness in most of the samples was below the CLT. Increasing the periods of MQWs most likely increased total strain energy, and as a result, induced MDs. Therefore, we should consider not only the CLT of each QW, but also the CLTs of the entire MQWs.

B. Structure model: Representing InGaN/GaN MQWs as InGaN single layers

As discussed in Sec. III, TEM measurements for a $(11\bar{2}2)$ InGaN/GaN MQW revealed that the MDs were introduced at the interface between the first InGaN QW and the underlying GaN, even if each QW was not relaxed. Similar phenomena have been observed in other material systems, such as InGaAs/GaAs MQWs,[30,31] SiGe/Si superlattices,[32] and InAsP/InGaAsP MQWs.[33]

We will now discuss why MDs were induced at the interface between the first InGaN QW and the underlying GaN. For this, we consider the strain energy stored in a MQW structure. Suppose MDs are introduced at a certain InGaN/GaN interface. In this situation, the MQW region above the interface is free-standing from the GaN substrate, but is coherent within the region, whereas the MQW region below the interface is still coherent to the substrate. The coherent region below the interface has more strain energy than the free-standing region. Therefore, it is the most energetically favorable to not have a coherent region, that is, to have MDs form at the interface between the bottom InGaN QW and the underlying GaN, as long as each QW thickness is below its CLT.

Based on the discussion above, we propose to treat InGaN/GaN MQWs as InGaN single layers characterized by the total thicknesses and the effective In compositions. Let us now consider how to determine the effective In composition. When a MQW (or superlattice) composed of any two kinds of layers becomes free-standing, one layer accommodates compressive stress, and the other accommodates tensile stress. These stresses can be transformed into the forces acting on the corresponding layers by multiplying the layer thicknesses.[24] The in-plane lattice parameter of a free-standing MQW can be determined when these forces with opposite sign are in equilibrium. For $(11\bar{2}2)$ InGaN/GaN MQWs, the balance of forces in the $[\bar{1}\bar{1}23]$ direction should be considered, because the lattice relaxation preferentially occurs in this direction. The equation for the balance is expressed as

$$\sigma_{\mathrm{w}}^{\mathrm{fs}} h_{\mathrm{w}} + \sigma_{\mathrm{b}}^{\mathrm{fs}} h_{\mathrm{b}} = 0, \tag{21}$$

where $\sigma_{\mathrm{i}}^{\mathrm{fs}}$ (i = w or b) is the in-plane stress in the $[\bar{1}\bar{1}23]$ direction when the MQW is free-standing, and h_{i} is the layer thickness. The subscripts w and b stand for QW and barrier layer, respectively. Because $\sigma_{\mathrm{i}}^{\mathrm{fs}}$ is a function of the in-plane lattice parameter, Eq. (21) determines it. Then, the effective In composition of a free-standing MQW is assumed to be the same as the In composition of an unstrained InGaN layer with the same in-plane lattice parameter.

We considered the force balance condition in the above discussion. However, note that the same in-plane lattice parameter can also be extracted from the condition that the strain energy is minimized. This is because the force acting on the crystal lattice is given by the differential of the strain energy, and consequently, the force balance and the energy minimum conditions are equivalent.

C. CLTs of $(11\bar{2}2)$ InGaN/GaN MQWs

Figure 6 shows how the effective In composition and the total thickness evolve during growth of an InGaN/GaN MQW, which is the same MQW as that in Fig. 3(b). The CLT calculated with Eq. (15) is also plotted. When the first InGaN QW is grown on a GaN substrate, the effective In composition does not change, whereas only the total thickness is increased as represented by (i) in Fig. 6. Next, during the growth of the subsequent GaN barrier layer, the effective In composition decreases, and the total thickness increases [(ii)]. Then, as the number of QW grows, such variations are repeated and the effective In composition approaches that of the entire MQW structure.

The dashed line represents the calculated CLT for InGaN single layer, using Eq. (15). The first InGaN QW is below the CLT, but during the growth of the second InGaN QW, the total thickness exceeds the CLT of MQW. This means that the SQW can be grown coherently, whereas the MQWs with a period of more than one may experience lattice relaxation, and MDs are introduced at the interface between the first InGaN QW and the underlying GaN, consistent with Figs. 3(a) and 3(b). That is, the prediction is that MDs can be induced when the total thickness of MQWs exceeds the calculated CLT at a certain growth stage.

To verify our model, we plot the experimentally assessed lattice relaxation in Fig. 7 as functions of the effective In composition and the total thickness of $(11\bar{2}2)$ InGaN/GaN MQWs. It is found that the experimental results can well be reproduced by Eq. (15), indicating that our method can be applied to the calculation of CLTs for $(11\bar{2}2)$ InGaN/GaN MQWs. To obtain high quality MQWs without MDs, the thickness of each QW should be below the CLT, as shown in Fig. 3(a), and the total thickness of MQW should not exceed the CLT determined as a function of the effective In composition, as shown in Fig. 7.

In this study, the experimental results for only the $(11\bar{2}2)$ InGaN/GaN MQWs were demonstrated. However,

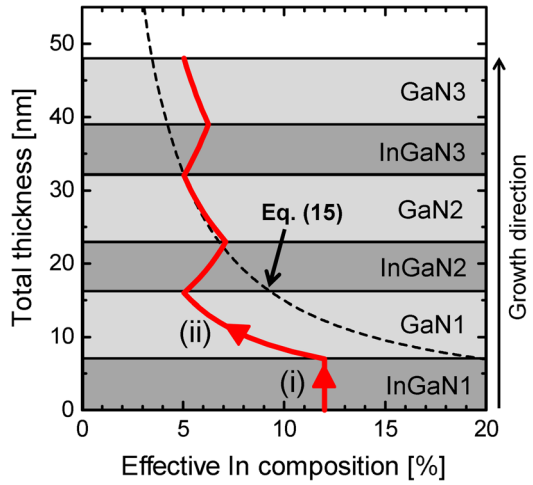

FIG. 6. Trace of effective In composition and total thickness during growth of an InGaN/GaN MQW. The dashed line represents CLT calculated with Eq. (15).

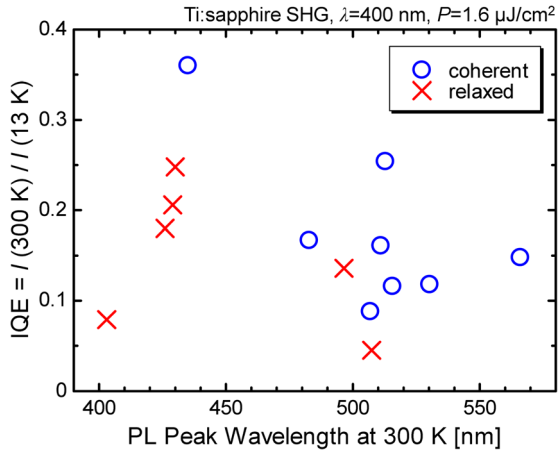

FIG. 8. IQEs of undoped InGaN/GaN QWs, as a function of PL peak wavelength. Open circles and crosses are for coherently grown and strain-relaxed $(11\bar{2}2)$ InGaN QWs, respectively.

the concept may be applied to nitride semiconductor heterostructures with various crystal orientations, and furthermore, to other material systems.

D. IQEs of $(11\bar{2}2)$ InGaN QWs

Because MDs may work as nonradiative recombination canters, we compared the optical properties of coherently grown and strain-relaxed $(11\bar{2}2)$ InGaN QWs. To evaluate the IQEs of the InGaN QWs, temperature-dependent photoluminescence (PL) measurements were performed. The excitation source was a frequency-doubled Ti:sapphire laser with a wavelength of 400 nm, a pulse width of 2 ps, a repetition rate of 80 MHz, and an excitation power density of 1.6 μJ/cm^2. In this study, IQE was defined as the integrated PL intensity at 300 K divided by that at 13 K.

Figure 8 shows the IQEs of $(11\bar{2}2)$ InGaN QWs at 300 K as a function of PL peak wavelength. Open circles and crosses indicate IQEs of coherently grown and strain-relaxed InGaN QWs, respectively. IQEs of coherently grown InGaN QWs tend to be larger than those of strain-relaxed InGaN QWs, as expected. Further improvement of IQEs may be achieved by optimizing the growth conditions to eliminate nanoscale nonradiative recombination centers, such as point defects and unexpected impurities.

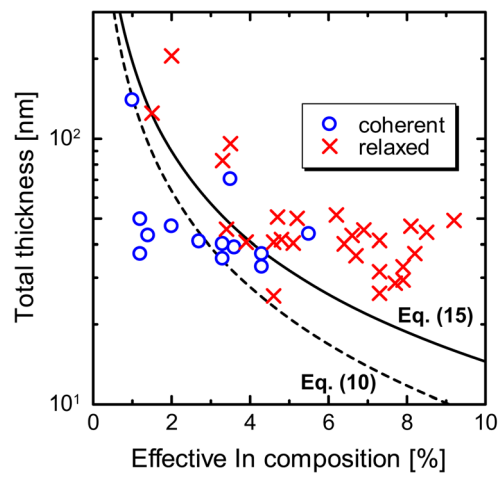

FIG. 7. Theoretical and experimental assessment of strain relaxation for InGaN/GaN MQWs as functions of effective In composition and total thickness. Solid and dashed lines are the CLTs calculated with Eqs. (15) and (10), respectively. Open circles and crosses are for coherently grown and strain-relaxed samples, respectively.

VI. CONCLUSION

We investigated the lattice relaxation in InGaN single layers, InGaN/GaN SQWs, and MQWs grown on the semipolar $(11\bar{2}2)$ GaN substrates. To reproduce experimentally revealed anisotropic lattice relaxation, the formulae of CLTs for anisotropic systems were developed, based on the force-balance model. TEM analyses of relaxed MQWs revealed that MDs were introduced at the interface between the first InGaN QW and the underlying GaN. Therefore, we propose to treat InGaN/GaN MQWs as InGaN single layers with the effective In compositions. The calculated CLTs were in reasonable agreement with the experimental results, verifying our approach. The achievement enabled us to design and fabricate high quality InGaN/GaN QWs without MDs. In fact, we confirmed that the IQEs of coherently grown InGaN QWs tended to be larger than those of strain-relaxed InGaN QWs.

ACKNOWLEDGMENTS

This work is partially supported by a Grant-in-Aid for Scientific Research and the Global COE Program by the Ministry of Education, Culture, Sports, Science, and Technology of Japan.

[1]S. H. Park and S. L. Chuang, Phys. Rev. B **59**, 4725 (1999).
[2]T. Takeuchi, H. Amano, and I. Akasaki, Jpn. J. Appl. Phys., Part 1 **39**, 413 (2000).
[3]K. Nishizuka, M. Funato, Y. Kawakami, Sg. Fujita, Y. Narukawa, and T. Mukai, Appl. Phys. Lett. **85**, 3122 (2004).
[4]M. Ueda, K. Kojima, M. Funato, Y. Kawakami, Y. Narukawa, and T. Mukai, Appl. Phys. Lett. **90**, 171907 (2007).
[5]H. Shen, M. Wraback, H. Zhong, A. Tyagi, S. P. DenBaars, S. Nakamura, and J. S. Speck, Appl. Phys. Lett. **94**, 241906 (2009).
[6]M. Funato, M. Ueda, D. Inoue, Y. Kawakami, Y. Narukawa, and T. Mukai, Appl. Phys. Express **3**, 071001 (2010).

[7]M. Funato, M. Ueda, Y. Kawakami, Y. Narukawa, T. Kosugi, M. Takahashi, and T. Mukai, Jpn. J. Appl. Phys., Part 2 **45**, L659 (2006).
[8]H. Sato, A. Tyagi, H. Zhong, N. Fellows, R. B. Chung, M. Saito, K. Fujito, J. S. Speck, S. P. DenBaars, and S. Nakamura, Phys. Status Solidi (RRL) **1**, 162 (2007).
[9]Y. Enya, Y. Yoshizumi, T. Kyono, K. Akita, M. Ueno, M. Adachi, T. Sumitomo, S. Tokuyama, T. Ikegami, K. Katayama, and T. Nakamura, Appl. Phys. Express **2**, 082101 (2009).
[10]S. Srinivasan, L. Geng, R. Liu, F. A. Ponce, Y. Narukawa, and S. Tanaka, Appl. Phys. Lett. **83**, 5187 (2003).
[11]D. Holec, P. M. F. J. Costa, M. J. Kappers, and C. J. Humphreys, J. Cryst. Growth **303**, 314 (2007).
[12]D. Holec, Y. Zhang, D. V. S. Rao, M. J. Kappers, C. McAleese, and C. J. Humphreys, J. Appl. Phys. **104**, 123514 (2008).
[13]M. Zhu, S. You, T. Detchprohm, T. Paskova, E. A. Preble, D. Hanser, and C. Wetzel, Phys. Rev. B **81**, 125325 (2010).
[14]A. Tyagi, F. Wu, E. C. Young, A. Chakraborty, H. Ohta, R. Bhat, K. Fujito, S. P. DenBaars, S. Nakamura, and J. S. Speck, Appl. Phys. Lett. **95**, 251905 (2009).
[15]A. E. Romanov, E. C. Young, F. Wu, A. Tyagi, C. S. Gallinat, S. Nakamura, S. P. DenBaars, and J. S. Speck, J. Appl. Phys. **109**, 103522 (2011).
[16]F. Wu, A. Tyagi, E. C. Young, A. E. Romanov, K. Fujito, S. P. DenBaars, S. Nakamura, and J. S. Speck, J. Appl. Phys. **109**, 033505 (2011).
[17]Z. H. Wu, T. Tanikawa, T. Murase, Y. Y. Fang, C. Q. Chen, Y. Honda, M. Yamaguchi, H. Amano, and N. Sawaki, Appl. Phys. Lett. **98**, 051902 (2011).
[18]S. Yoshida, T. Yokogawa, Y. Imai, S. Kimura, and O. Sakata, Appl. Phys. Lett. **99**, 131909 (2011).
[19]J. W. Matthews and A. E. Blakeslee, J. Cryst. Growth **27**, 118 (1974).
[20]R. People and J. C. Bean, Appl. Phys. Lett. **47**, 322 (1985).
[21]A. Fischer, H. Kühne, and H. Richter, Phys. Rev. Lett. **73**, 2712 (1994).
[22]M. Funato, D. Inoue, M. Ueda, Y. Kawakami, Y. Narukawa, and T. Mukai, J. Appl. Phys. **107**, 123501 (2010).
[23]D. Hull and D. J. Bacon, *Introduction to Dislocations*, 4th ed. (Butterworth-Heinemann, Oxford, 2001).
[24]J. P. Hirth and J. Lothe, *Theory of Dislocations*, 2nd ed. (McGraw-Hill, New York, 1985).
[25]A. Fischer, H. Kühne, M. Eichler, F. Holländer, and H. Richter, Phys. Rev. B **54**, 8761 (1996).
[26]L. J. Teutonico, Mater. Sci. Eng. **6**, 27 (1970).
[27]J. F. Nye, *Physical Properties of Crystals* (Oxford Science, New York, 1957).
[28]I. Vurgaftman and J. R. Meyer, J. Appl. Phys. **94**, 3675 (2003).
[29]P. S. Hsu, E. C. Young, A. E. Romanov, K. Fujito, S. P. DenBaars, S. Nakamura, and J. S. Speck, Appl. Phys. Lett. **99**, 081902 (2011).
[30]D. J. Dunstan, S. Young, and R. H. Dixon, J. Appl. Phys. **70**, 3038 (1991).
[31]R. Hull, J. C. Bean, F. Cerdeira, A. T. Fiory, and J. M. Gibson, Appl. Phys. Lett. **48**, 56 (1986).
[32]D. C. Houghton, D. D. Perovic, J.-M. Baribeau, and G. C. Weatherly, J. Appl. Phys. **67**, 1850 (1990).
[33]M. Ogasawara, H. Sugiura, M. Mitsuhara, M. Yamamoto, and M. Nakao, J. Appl. Phys. **84**, 4775 (1998).